Modeling the Diffusion-Free Liquid Phase Residence Time Distribution of Taylor Flow by the Unit Cell Concept: Progress and Limitations

Sercan Erdogan[a,b], Martin Wörner[a,*], Hakan Serhad Soyhan[c]

[a] Karlsruhe Institute of Technology (KIT), Institute for Nuclear and Energy Technologies, Hermann-von-Helmholtz-Platz 1, 76344 Eggenstein-Leopoldshafen, Germany

[b] Mechanical Engineering Department, Institute of Natural Sciences, Sakarya University, Esentepe Campus, 54187 Sakarya, Turkey

[c] Mechanical Engineering Department, Faculty of Engineering, Sakarya University, Esentepe Campus, 54187 Sakarya, Turkey

* Correspondence concerning this article should be address to M. Wörner

E-mail: martin.woerner@kit.edu, Phone +49 721 608 24477, Fax: +49 721 608 24837

Abstract

In this paper we study the diffusion-free liquid phase residence time distribution (RTD) of laminar Taylor flow in square mini-channels numerically and analytically. We evaluate the RTD caused by the non-uniform laminar velocity field for co-current upward and downward Taylor flow from detailed numerical simulations obtained with a volume-of-fluid method by diffusion-free Lagrangian tracking of a set of virtual particles. The numerical RTD curves are used to develop a compartment model for the RTD of a Taylor flow unit cell (which consists of one gas bubble and one liquid slug) in the fixed frame of reference. While the new model is conceptually similar to models from literature, it is refined with respect to (i) the delay time (i.e. the residence time of the fastest liquid elements, modeled by a plug flow reactor) and (ii) the difference in slope of the RTD at small and large residence times (modeled by two parallel continuous stirred tank reactors with different mean residence time). It is shown that the refined model fits the numerical unit cell RTD reasonably well for different flow conditions. From the unit cell RTD model, the RTD for two and three unit cells in series is computed by a convolution procedure. The agreement between the numerical and the convolution-based RTD for multiple unit cells is not satisfactory and indicates the inappropriateness of the convolution procedure for computing the diffusion-free RTD of multiple unit cells in Taylor flow. The failure of the convolution procedure is attributed to the dividing streamline, which separates in Taylor flow the liquid phase in two regions, one with recirculating and one with bypass flow. In the absence of diffusion, the diving streamline is never crossed. As a consequence, locations of tracer particles in neighboring unit cells are not independent which invalidates the unit cell convolution approach.

Keywords: Residence time distribution; Taylor flow; Bubble train flow; Numerical simulation; Unit cell; Compartment model; Convolution

Nomenclature

C	tracer concentration (mol/m^3)
C_{cs}	ratio between mean and maximum velocity in laminar channel flow
Ca	capillary number
d_B	bubble diameter at a certain axial position (m)
$d_{B,max}$	maximum bubble diameter (m)
d_h	hydraulic diameter of channel (m)
D	molecular diffusion coefficient of tracer in liquid phase (m^2/s)
E	residence time distribution (1/s)
h_F	thickness of liquid film between gas bubble and channel wall (m)
J	total superficial velocity (m/s)
J_G	superficial velocity of gas phase (m/s)
J_L	superficial velocity of liquid phase (m/s)
L_{ref}	reference length scale (m)
L_S	liquid slug length (m)
L_{travel}	axial travelling distance of particles to determine the RTD (m)
L_{UC}	length of unit cell (m)
n	number of CSTRs or unit cells in series
N_{cross}	number of unit cells particles must travel to obtain the RTD
N_P	number of particles
Pe	Peclet number
Q	volumetric flow rate (m^3/s)
Re_B	bubble Reynolds number
t	time (s)
t_{ref}	reference time scale (s)
Δt	time step width (s)
Δt_{class}	time interval of classes in the RTD (s)
U_B	bubble velocity (m/s)
U_F	mean velocity in liquid film at a certain axial position (m/s)
U_L	mean liquid velocity in the computational domain (m/s)
$U_{L,max}$	maximum axial velocity in the liquid slug (m/s)
$U_{L,max}^{fd}$	maximum axial velocity in fully developed Poiseuille flow (m/s)
U_{ref}	reference velocity scale (m/s)
V	volume (m^3)
Δx	mesh size (m)

Greek symbols

α	weighting factor in PDD model
β	pre-factor of maximum bubble diameter in PDD model
δ	Dirac delta function
ε	gas volume fraction in the unit cell
λ	ratio $U_{\mathrm{L,max}} / U_{\mathrm{L,max}}^{\mathrm{fd}}$
μ	dynamic viscosity (Pa s)
ρ	density (kg/m^3)
σ	coefficient of surface tension (N/m)
τ	mean residence time (s)
τ_{B}	bubble break through time (s)
τ_{D}	delay time (s)
τ_{F}	mean residence time of liquid film/corner flow (s)
τ_{h}	mean hydrodynamic residence time (s)
τ_{S}	mean residence time of liquid slug (s)

Subscripts

B	bubble
F	liquid film
G	gas phase
L	liquid phase
p	particle
ref	reference value
S	liquid slug
UC	unit cell

Abbreviations

CSTR	continuous stirred tank reactor
PD	peak-decay
PDD	peak-decay-decay
PFR	plug flow reactor
RTD	residence time distribution

1. Introduction

Segmented gas-liquid flow is a common two-phase flow pattern in narrow channels. It is also denoted as Taylor flow or bubble train flow and consists of a sequence of elongated gas bubbles which almost fill the entire channel cross section (Taylor bubbles). The individual bubbles move along the channel while they are separated by liquid slugs. Taylor flow is of technical relevance e.g. for miniaturized multiphase reactors [1-5] and multiphase monolith reactors [6-8]. It has been considered for production of H_2O_2 [9] and is finding increasing interest for potential use in Fischer-Tropsch synthesis [10-13].

In Taylor flow, the length of the liquid slugs and the size of individual bubbles underlie variations. The variation of the bubble size results in a variation of the translational velocity of individual bubbles. This may lead to coalescence and thus a further change of the bubble size and slug length distribution. A useful abstraction of real Taylor flow is *perfect Taylor flow*, where the bubbles are assumed to have identical size, shape and velocity and where the length of all liquid slugs is the same. Then, the hydrodynamics of Taylor flow is fully described by a unit cell (UC) which consists of one bubble and one liquid slug.

For the design and optimization of micro-structured chemical reactors, the ability to reliably predict the RTD is of great importance. In Taylor flow, the RTD of the continuous liquid phase is of major interest, since the variation of the residence time of the gas phase is small and its mean value is given by the ratio between channel length and bubble velocity. Desirable is a plug flow behavior of the liquid phase with a narrow RTD. Sun et al. [14] recently investigated the influence of the RTD on the synthesis of biodiesel in capillary micro-reactors operated with Taylor flow. They found that the RTD in the micro-channel reactor was remarkably decreased compared to the RTD which is required in batch systems to obtain a high yield under the same reaction conditions. However, the RTD of the micro-reactors had to be controlled to avoid the saponification of the biodiesel. While this example demonstrates the practical importance of the RTD, there are, unfortunately, only very few experimental data on the liquid phase RTD available in literature for miniaturized multiphase reactors

such as monolith reactors. This may be attributed on one hand to the difficulties of performing local measurements of the RTD in narrow channels and on the other hand to the only recently increasing interest in this topic. As a consequence, reliable and validated general models for the RTD in multi-phase micro-structured reactors are missing. This is in particular true for channels of non-circular cross-section, which are quite common in monoliths and micro-structured reactors. In rectangular channels, the film thickness at the circumference of the bubble is not constant. The resulting so-called corner flow can be significant [15] and makes the application of RTD models for circular channels inappropriate.

In experiments the RTD is often measured by a stimulus-response technique, where a specific quantity of a tracer is introduced at the system inlet as a short duration pulse or a step function and where the time variation of the tracer concentration is recorded at the outlet. This procedure is well suited for macro-reactors, where the reactor volume is much larger than the volume of the tracer measurement device. However, for micro-structured reactors, the reactor volume is usually smaller than the volume of the measuring unit. This means that the response of the tracer may already be influenced by the measurement configuration itself. Therefore, for RTD measurements in small channels optical methods should be preferred which measure directly inside the channel. Measurements of the liquid phase RTD in two-phase flow through narrow channels or monolith reactors are reported in [2, 16-24]. As compared to single phase flow, the RTD of Taylor flow is very narrow [24], which is a distinct advantage.

An alternative way to determine the RTD is by means of computational fluid dynamics (CFD). There exist two principle options. The first one is the numerical simulation of the stimulus-response experiment, i.e. setting a short concentration pulse at the inlet of the computational domain, computing the unsteady concentration field of the tracer within the domain and evaluating it at the outlet. This approach has been used in a modified form in [25, 26] to determine the reactor residence time for Taylor flow in a circular micro-channel from the RTD of a single unit cell by a convolution procedure. The second possibility is the particle tracking method. Here, virtual particles are released at the inlet and are advected by the local velocity field which is interpolated from the Eulerian grid. Molecular

diffusion can be modeled by a random walk of the tracer particles [27-30]. The relative importance of advective and diffusive transport is characterized by the Peclet number $Pe = U_B d_h / D$. Here, U_B is the bubble velocity, d_h the hydraulic diameter of the channel and D the molecular diffusion coefficient of the tracer in the liquid phase. The RTD obtained by a particle tracking method that does not take into account molecular diffusion is representative for an infinite value of the Peclet number.

An overview on models for the RTD in Taylor flow can be found in [15, 31]. Early studies by Thiers et al. [32] and Snyder and Adler [33, 34] aimed to predict axial dispersion in segmented flow through tubes in order to support the optimal design of continuous flow analyzers. In [32] perfect mixing between the slugs and the film is assumed and a tank-in-series model connected by the film surrounding the bubbles is derived. Pedersen and Horvath [35] developed a two-region model consisting of the recirculating liquid bulk and the liquid film. Both regions are assumed perfectly mixed and the transfer between both is modeled by an adjustable mass transfer coefficient. Salman et al. [36] developed a numerical model for predicting the RTD of Taylor flow which is valid for low values of Pe. The model assumes liquid slugs of uniform concentration and liquid films around the bubble that can be adequately described by a one-dimensional convection-diffusion equation. For values $Pe > 10$ the model can be simplified and an analytical solution is derived, which represents the RTD of a unit cell by a tank-in-series model, consisting of a plug flow reactor (PFR) and a continuous stirred tank reactor (CSTR). In a more recent paper, Salman et al. [26] numerically evaluated RTDs for a wide range of Peclet numbers and compared it with predictions from three literature models (CSTR-PFR model, two-region model [35], and the model of Thulasidas et al. [16]). They found that the shape of the RTD and the performance of the different models strongly depend on $U_B h_F / D$, i.e. the Peclet number based on the liquid film thickness h_F between the bubble and the channel wall. Muradoglu and co-workers performed extensive two-dimensional computational studies on the axial dispersion in segmented gas liquid flow in straight [27] and serpentine channels [28, 37]. They considered a frame of reference moving with one segment (which consists of two half bubbles and one liquid slug) and investigated in detail the effect of Peclet number, capillary number and segment size. For high Peclet numbers a model for the tracer concentration in the i-th segment is proposed which involves the liquid

film thickness as main parameter. Wörner et al. [38] developed a particle method for evaluating the liquid phase RTD from detailed numerical simulations and gave results for the diffusion-free RTD in co-current upward Taylor flow in a square mini-channel (d_h = 2 mm). Similar to [36], the unit cell RTD is modeled by the PFR-CSTR in series compartment model. In practice, a channel with Taylor flow contains tens or hundreds of unit cells. A common approach is to compute the RTD of the entire channel from the RTD of the unit cell by means of a convolution method, see e.g. [26, 35].

The general motivation of this paper is to contribute to the development of models that can predict the RTD in Taylor flow from given fluid properties and known integral flow parameters such as the superficial velocities of the phases only. Unlike other studies from literature, we restrict ourselves first to the case of the diffusion free RTD, i.e. the RTD that is caused by the spatially non-uniform velocity distribution of the Taylor flow (limit $Pe \to \infty$). If this diffusion free RTD can be properly modeled in a mechanistic way for different hydrodynamic conditions, then in a second step the model can be extended to account for the effect of diffusion. In this context, the present paper has two specific objectives. First, we refine the unit cell RTD model from [38] to be valid also for downward flow and second, test if the diffusion-free RTD for a number of unit cells in series can be reliably predicted from the unit cell RTD model by a convolution procedure. In section 2 we present RTD compartment models for a single Taylor flow unit cell and discuss issues related to the numerical simulation of Taylor flow and the numerical evaluation of the RTD. Section 3 is devoted to the analytical modeling of the diffusion-free RTD in Taylor flow. This section covers the development of a refined unit cell model, a model for multiple unit cells and the discussion of the results. In section 4 we present the conclusions.

2. Theory and numerical method

2.1. Compartment RTD models for a single Taylor flow unit cell

The differential RTD of a chemical reactor, $E(t)$, is a probability distribution function that describes the amount of time that fluid elements spend inside the reactor [39, 40]. For laminar channel flow, the RTD often shows a characteristic behavior, namely $E(t)$ is zero for small values of t,

becomes positive at the delay time τ_D (also denoted as first appearance time) where it has its highest value and decreases towards zero for very large values of t. This behavior can be described by a PFR-CSTR in series compartment model (see sketch in Fig. 1) whose RTD is [39]

$$E_{\text{PFR-CSTR}}(t) = \begin{cases} 0 & \text{for } t < \tau_{\text{PFR}} \\ \dfrac{1}{\tau_{\text{CSTR}}} \exp\left(-\dfrac{t - \tau_{\text{PFR}}}{\tau_{\text{CSTR}}} \right) & \text{for } t \geq \tau_{\text{PFR}} \end{cases} \tag{1}$$

Here, τ_{PFR} and τ_{CSTR} are the mean residence time of the PFR and CSTR, respectively.

Salman et al. [36] adopted this concept to model the liquid phase RTD of a Taylor flow unit cell. The PFR corresponds to the delay time, i.e. the residence time of the fastest liquid fluid elements, which is modeled as

$$\tau_{\text{PFR}} \triangleq \tau_D = \frac{L_B}{U_B} \tag{2}$$

Due to the recirculation, the liquid in the slug is well mixed [41], so that each slug can be considered as a CSTR. In [36] the mean residence time of the liquid slug is modeled as

$$\tau_{\text{CSTR}} \triangleq \tau_S = \frac{V_S / A_F}{U_B} \tag{3}$$

In the latter two equations, L_B is the bubble length, V_S the volume of the liquid slug, and A_F the cross-sectional area of the liquid film. Wörner et al. [38] evaluated the diffusion-free liquid phase unit cell RTD from numerical simulations of co-current upward Taylor flow in a square mini-channel and found that the model in [36] underestimates τ_D and overestimates the steepness of the exponential decay. In [38] the delay time is modeled by the bubble break-through time

$$\tau_D \triangleq \tau_B = \frac{L_{UC}}{U_B} \tag{4}$$

This is the time the bubble needs to cover a distance of one unit cell length L_{UC}. For the mean residence time of the liquid slug two different models are proposed in [38], namely $\tau_S = L_{UC} / U_L$ and $\tau_S = L_{UC} / J$, respectively. Here, $J = J_G + J_L = \varepsilon U_B + (1-\varepsilon) U_L$ is the total superficial velocity, and U_L and ε denote the mean liquid velocity and gas volume fraction in the computational domain,

respectively. For the remainder of the paper we will denote the model with $\tau_S = L_{UC} / J$ and $\tau_D = \tau_B$ as WGO model (according to the initials of the three authors of [38]).

(Approximate location for Fig. 1)

2.2. Numerical simulation of Taylor flow

In this paper we compare analytical RTD models with RTD data evaluated from detailed numerical simulations. These are performed with an in-house computer code [42-45], which uses an interface reconstructing volume-of-fluid method to solve the single-field Navier-Stokes equations with surface tension term for two incompressible immiscible fluids with constant fluid properties (i.e. density, viscosity, surface tension) in non-dimensional form. The code has been comprehensively validated, both by test problems and by experiments. An example is the planar Bretherton problem, where the computed liquid film thickness is in excellent agreement with analytical and numerical results for a wide range of capillary numbers [45]. For upward Taylor flow in a square mini-channel (d_h = 2 mm) a comprehensive code-to-code comparison with three major commercial CFD codes was performed indicating a good performance of the in-house code [46]. For co-current downward Taylor flow in a square mini-channel (d_h = 1 mm) very good agreement with experimental bubble shape visualizations is obtained for different flow rates [47].

The set-up of the simulations for Taylor flow in a square mini-channel is described in [38, 44] and is only shortly repeated here. The co-ordinate system is Cartesian and the computational domain is a rectangular box. At the four channel side walls no-slip boundary conditions are applied while in (vertical) axial direction (y) periodic boundary conditions are used. The simulations start from fluid at rest with a bubble placed in the center of the computational domain and are continued until U_B and U_L are constant in time. The bubble volume corresponds to a gas holdup ε of about 33%. The channel cross-section is square with hydraulic diameter $d_h = 2\,\mathrm{mm}$. The reference length and velocity

scale that are used to normalize the governing equations are $L_{\mathrm{ref}} = d_{\mathrm{h}}$ and $U_{\mathrm{ref}} = 0.0264\,\mathrm{m/s}$, respectively, resulting in the reference time scale $t_{\mathrm{ref}} = L_{\mathrm{ref}} / U_{\mathrm{ref}} = 0.0757\,\mathrm{s}$. The physical properties of the phases are $\rho_{\mathrm{L}} = 957\ \mathrm{kg/m^3}$, $\rho_{\mathrm{G}} = 11.7\ \mathrm{kg/m^3}$, $\mu_{\mathrm{L}} = 0.048\ \mathrm{Pa \cdot s}$, $\mu_{\mathrm{G}} = 0.184\ \mathrm{mPa \cdot s}$, and $\sigma = 0.02218\,\mathrm{N/m}$. For these conditions, three cases are considered in this paper which differ with respect to the value of L_{UC} and the flow direction, see Tab. 1. Case A and B are for co-current upward flow and correspond to case A2 and E in [38], respectively, while case C is for co-current downward flow. In all cases the grid is uniform with mesh size $\Delta x = L_{\mathrm{ref}} / 48$ which is sufficiently fine as demonstrated by a grid refinement study, see [38]. In Tab. 1 various parameters of the three cases are listed. Note that for all cases the capillary number is about 0.2 so that the bubble shape is axi-symmetric, i.e. its cross-section at any axial position is circular.

(Approximate location for Tab. 1)

2.3. Numerical evaluation of the diffusion-free RTD in Taylor flow

Wörner et al. [38] developed a method for evaluating the (diffusion-free) liquid phase RTD in a Taylor flow unit cell from the instantaneous three-dimensional velocity and volume fraction field, provided by a detailed numerical simulation. The method relies on the introduction of a set of equidistantly distributed virtual tracer particles in the volume occupied by the liquid phase within a single flow unit cell. The RTD is obtained by statistical evaluation of the time required by the particles to travel an axial distance L_{UC}, and by an appropriate weighting procedure which takes into account the axial velocity at the initial particle position in order to obtain the “mixing cup” RTD [48]. The method is only useful for fully developed Taylor flow, where U_{B} is constant and the bubble shape and the velocity field are steady in a frame of reference moving with the bubble. The method for evaluation of the RTD involves three parameters. The first parameter is the particle Courant-Friedrich-Levy number $CFL_{\mathrm{p}} = \Delta t_{\mathrm{p}} \left| \mathbf{u}_{\mathrm{p}} \right| / \Delta x$ which determines the time step width Δt_{p} that is used for the particle tracking (here it is $CFL_{\mathrm{p}} = 0.2$).

The second parameter N_P defines the number of particles per unit length. It determines the distance between neighboring particles in the three coordinate directions and thus the initial positions of the particle set. Here, we use $N_\mathrm{P} = 48$. With this value the number of particles released in the liquid phase ranges from 69 883 (case A) to 123 663 (case B), depending on the length of the unit cell. An increase of N_P (and thus the number of particles that are released in the liquid) has only a very small effect on the RTD. Essentially, it only increases the value of the largest recorded particle residence time. This is because the increase of N_P is associated with a decrease of the distance between the initial positions of the particles. Thus, some particles are initially located closer to the no-slip wall. These are advected with a smaller velocity and need more time to travel an axial distance L_UC which results, therefore, in larger residence times. We evaluated the variance of the numerical RTD for different values of N_P and found that the variance is finite and strongly increases with increasing number of particles. This is a direct consequence of the lower wall distance of some particles and the associated longer residence time. It is well known, that in the absence of diffusion the variance of the RTD in laminar flow is infinite [49]. This behavior is thus correctly captured by our numerical RTD evaluation procedure as N_P increases.

The third parameter is Δt_class and serves to create a suitable histogram from the set of traveling times of all particles. It divides the time axis in equal sized intervals denoted as classes. By sorting the residence time of all particles in classes and subsequent normalization of the resulting histogram, the RTD is obtained. Since the particle traveling times are discrete real numbers, in the limit of $\Delta t_\mathrm{class} \to 0$ rather spiky and discontinuous histograms result, where most of the classes are empty (because for a finite number of particles no travel time falls in these tiny intervals). Fig. 2 illustrates the influence of Δt_class on the numerical RTD curve for case C. It is evident that $\Delta t_\mathrm{class} = \tau_\mathrm{D}/3$, $\tau_\mathrm{D}/2$ and τ_D, respectively, yield quite different values of E in neighboring classes. Increasing the value of Δt_class smoothes the RTD curve, but decreases the resolution and lowers the height of the peak value. However, the area of the first three non-zero classes for $\Delta t_\mathrm{class} = \tau_\mathrm{D}/3$, the area of the first two non-zero classes for $\Delta t_\mathrm{class} = \tau_\mathrm{D}/2$ and the area of the first non-zero class for $\Delta t_\mathrm{class} = \tau_\mathrm{D}$ are all equal, see

Fig. 2. Nevertheless, the sensitivity of the numerical RTD curve with respect to $\Delta t_{\mathrm{class}}$ makes an objective comparison with analytical RTD models somewhat difficult.

A particle that leaves the computational domain through one of the two faces with periodic boundary conditions re-enters it through the opposite face. Thus a particle may travel an axial distance that is larger than the length of the computational domain. We define the axial distance that any virtual particle must travel before its residence time is recorded by $L_{\mathrm{travel}} = N_{\mathrm{cross}} L_{\mathrm{UC}}$, where $N_{\mathrm{cross}} \in \mathbb{N}$. We checked that the RTD evaluated from case A with $N_{\mathrm{cross}} = 2$ is the same as RTD evaluated with $N_{\mathrm{cross}} = 1$ from a case that is equivalent to case A, but contains two unit cells in the computational domain [50]. Thus, setting $N_{\mathrm{cross}} > 1$ allows evaluating the RTD for axial distances corresponding to multiple unit cells. In section 3.2, this procedure is used for evaluating the numerical RTD for 2 and 3 unit cells. Within a reasonable upper limit of Lagrangian time steps (which is here set to 300 000), all releases particles cross the domain for $N_{\mathrm{cross}} = 1$ and 2, whereas for $N_{\mathrm{cross}} = 3$ it are still more than 98%. In any case, no particle hits the wall.

(Approximate location for Fig. 2*)*

3. Model refinement and discussion

In this section we develop a refined analytical model for the diffusion-free liquid phase RTD in a Taylor flow unit cell and then utilize this model to obtain the RTD for a series of unit cells by a convolution procedure.

3.1.1. Modeling of the delay time

In Fig. 3 we compare the unit cell RTD of the WGO model (solid line) with the numerical RTD curve (shaded area) for case C. The dashed vertical line denotes the bubble break-through time. It is evident that some liquid needs less time than the bubble to pass the channel. Thus, this liquid moves with a velocity that is larger than U_{B}. Therefore, the bubble break-through time differs from the delay

time and a more general model for τ_D is required which accounts for the actual maximum liquid axial velocity in the unit cell.

(Approximate location for Fig. 3)

For any fully developed laminar flow through a straight channel there exists a linear relationship between the mean and maximum velocity of the form $U_{mean} = C_{cs} U_{max}$. The value of the constant C_{cs} depends on the shape of the channel cross-section and is e.g. $C_{cs} = 0.5$ for a circular and $C_{cs} = 0.477$ for a square channel [51]. In Taylor flow, the mean liquid velocity within the liquid slug is $U_{L,mean} = J$. Thus, if the liquid slug is long enough for the velocity profile to become fully developed, it is $U_{L,max}^{fd} = J / C_{cs}$. For shorter liquid slugs the maximum liquid velocity may be smaller, say $U_{L,max} = \lambda U_{L,max}^{fd}$ with $0 < \lambda \leq 1$. In Fig. 4 we show the profiles of the magnitude of the axial velocity in the middle of the liquid slug for the three cases; the horizontal lines denote the maximum velocity in a fully developed laminar flow with the same flow rate. It is evident that the velocity profiles are not parabolic but rather flat while the maximum velocity is smaller than $U_{L,max}^{fd}$. Thus, the liquid slug (whose length is smaller than d_h in all present cases) is too short for the velocity profile to become fully developed. This result is consistent with experiments [41, 52]; in [41] e.g. it is reported that the Poiseuille profile within the liquid slug is fully developed for $L_S / d_h \geq 1.5$.

(Approximate location for Fig. 4*)*

For the very short liquid slug of case A it is by incident $U_{L,max} \approx U_B$. For the longer liquid slugs of cases B and C, the velocity profile tends to become more parabolic and $U_{L,max}$ is larger than U_B so that modeling the delay time by the bubble break-through time is not appropriate. To obtain a more

general model for the delay time, which is valid for upward and downward flow and any length of the liquid slug, we set $\tau_{\mathrm{D}} = L_{\mathrm{UC}} / U_{\mathrm{L,max}}$. This yields together with $U_{\mathrm{L,max}} = \lambda U_{\mathrm{L,max}}^{\mathrm{fd}} = \lambda J / C_{\mathrm{cs}}$ the result

$$\tau_{\mathrm{D}} = \frac{C_{\mathrm{cs}}}{\lambda} \frac{L_{\mathrm{uc}}}{J} \tag{5}$$

In the following, we will denote the model with τ_{D} given by Eq. (5) and $\tau_{\mathrm{S}} = L_{\mathrm{UC}} / J$ as peak-decay (PD) model. This name reflects that the RTD consists of one peak followed by an exponential decay. In the PD model λ is a yet unknown function of $L_{\mathrm{S}} / d_{\mathrm{h}}$ which approaches unity for large values of $L_{\mathrm{S}} / d_{\mathrm{h}}$. In this paper, we take the values of λ evaluated from the numerical simulations which are in the range 0.86–0.88, see Tab. 1. The development of a suitable relationship for $\lambda = \lambda(L_{\mathrm{S}} / d_{\mathrm{h}})$ will be considered in future.

3.1.2. Tail of RTD

In Taylor flow the tail of the RTD corresponds to the flow in the liquid film which is almost stagnant. The inset graphic in Fig. 3 shows the numerical and modeled RTD in a semi-logarithmic representation. This allows for an easy visual comparison of the slopes of both RTDs. The numerical RTD shows two different slopes, a steeper one for $t / t_{\mathrm{ref}} < 5$ and a flatter one for $t / t_{\mathrm{ref}} > 5$. In contrast, the slope of the WGO model is constant and the tail of the RTD is not accurately represented by this model. In [38], the steeper RTD slope for $t / t_{\mathrm{ref}} < 5$ is better fitted by $\tau_{\mathrm{S}} = L_{\mathrm{UC}} / J$ than by $\tau_{\mathrm{S}} = L_{\mathrm{UC}} / U_{\mathrm{L}}$ because residence times $t / t_{\mathrm{ref}} < 5$ correspond mainly to fluid elements in the liquid slug, where the mean velocity is equal to J. However, the flatter slope for $t / t_{\mathrm{ref}} > 5$ is better approximated by $\tau_{\mathrm{S}} = L_{\mathrm{UC}} / U_{\mathrm{L}}$ than by $\tau_{\mathrm{S}} = L_{\mathrm{UC}} / J$. This is because residence times $t / t_{\mathrm{ref}} > 5$ correspond to fluid elements in the four corners of the channel. There, the mean liquid velocity is smaller than J and may be approximated by the mean liquid velocity U_{L}. However, as compared to the numerical RTD, the slope for $\tau_{\mathrm{S}} = L_{\mathrm{UC}} / U_{\mathrm{L}}$ is still slightly too steep for high residence times, see Fig. 8 a) in [38]. Hence, an even lower mean liquid velocity should be chosen for the film/corner flow to cause a flatter slope for high residence times.

One possibility to account for the different slopes of the RTD at small and large residence times is a three tank compartment model consisting of a PFR that is in series with two parallel CSTRs, see Fig. 5. The RTD of this compartment model is characterized by a peak which is followed by the superposition of two exponential decays with different slopes. Here, we denote this model as peak-decay-decay (PDD) model. In the PDD model one CSTR corresponds to the recirculating liquid slug region and the other one to the corner/film flow region. Since both CSTRs are in parallel, the resulting RTD is the sum of two exponentials. The slopes of both exponentials are determined by the mean residence times of the liquid slug $\tau_{\mathrm{S}} = L_{\mathrm{UC}} / J$ and the liquid film/corner flow $\tau_{\mathrm{F}} = L_{\mathrm{UC}} / U_{\mathrm{F}}$, where U_{F} denotes the mean velocity in the liquid film/corner flow. The RTD of the PDD model is

$$E_{\mathrm{UC}}^{\alpha}(t) = \begin{cases} 0 & \text{for } t < \tau_{\mathrm{D}} \\ \dfrac{\alpha}{\tau_{\mathrm{S}}} \exp\left(-\dfrac{t-\tau_{\mathrm{D}}}{\tau_{\mathrm{S}}} \right) + \dfrac{1-\alpha}{\tau_{\mathrm{F}}} \exp\left(-\dfrac{t-\tau_{\mathrm{D}}}{\tau_{\mathrm{F}}} \right) & \text{for } t \geq \tau_{\mathrm{D}} \end{cases} \tag{6}$$

Here, $0 < \alpha \leq 1$ is a weighting factor for the relative importance of the liquid slug and liquid film region. The mean residence time of the PDD model is $\tau_{\mathrm{UC}}^{\mathrm{PDD}} = \tau_{\mathrm{D}} + \alpha\tau_{\mathrm{S}} + (1-\alpha)\tau_{\mathrm{F}}$; the variance is $(\sigma^2)_{\mathrm{UC}}^{\mathrm{PDD}} = 2\alpha\tau_{\mathrm{S}}^2 + 2(1-\alpha)\tau_{\mathrm{F}}^2 - \left(\alpha\tau_{\mathrm{S}} + (1-\alpha)\tau_{\mathrm{F}}\right)^2$, which is finite. For $\alpha = 1$ the PDD model reduces to the PD model. At this stage, the PDD model involves two unknowns that must be modeled properly, namely α and U_{F}.

(Approximate location for Fig. 5)

A relation for U_{F} can be obtained from a liquid mass balance in a frame of reference moving with the bubble. We consider a control volume that consists of an axial portion of the channel where one end is in the liquid slug and the other end is in the bubble region. Then a balance of the liquid inflow and outflow flow rates yields

$$\left(J - U_{\mathrm{B}}\right) A = (U_{\mathrm{F}} - U_{\mathrm{B}})(A - A_{\mathrm{B}}) \tag{7}$$

In this equation, $U_{\mathrm{F}}(y)$ and $A_{\mathrm{B}}(y)$ represent the mean axial liquid velocity and bubble cross-sectional area, respectively, at an arbitrary position y which denotes the control volume outlet. For the cases considered in this paper the bubble is always axi-symmetric. Thus it is $A_{\mathrm{B}}(y)=\pi d_{\mathrm{B}}^2/4$, where $d_{\mathrm{B}}(y)$ denotes the local cross-sectional bubble diameter. For a square channel it is $A=d_{\mathrm{h}}^2$ and we obtain from Eq. (7) the result

$$U_{\mathrm{F}}(y)=U_{\mathrm{B}}-\left(U_{\mathrm{B}}-J\right)\left[1-\frac{\pi}{4}\left(\frac{d_{\mathrm{B}}(y)}{d_{\mathrm{h}}}\right)^2\right]^{-1} \tag{8}$$

The value of U_{F} in this relation is very sensitive to d_{B}. As pointed out in [53], U_{F} can be negative so that in regions where d_{B} is close to its maximum the net flow in the liquid film and gas bubble may be counter-current. The PDD model is, however, only reasonable for $\tau_{\mathrm{F}}>0$ and thus requires $U_{\mathrm{F}}>0$.We therefore define $d_{\mathrm{B}}=\beta d_{\mathrm{B,max}}$ with $0<\beta\le 1$. The bubble diameter $d_{\mathrm{B,max}}$ depends on the capillary number and can be determined from appropriate correlations, see e.g. [7]. Here, we take the values from Tab. 1. The value of β is debatable; as U_{F} should be representative for the entire liquid film, β should probably not be 1 but slightly smaller to ensure $U_{\mathrm{F}}>0$. To investigate the effect of β, we consider here two different values, namely 1 and 0.97. In Tab. 2 we list the values of U_{F} that are obtained from Eq. (8) for the different cases and both values of β.

We now determine a suitable model for the weighting factor α and consider two possible choices. In the first one, we compute α from relation

$$\alpha_{\mathrm{Q}}=\frac{Q_{\mathrm{L,S}}}{Q_{\mathrm{L,S}}+Q_{\mathrm{L,F}}}=\frac{Q_{\mathrm{L}}-Q_{\mathrm{L,F}}}{Q_{\mathrm{L}}} \tag{9}$$

By Eq. (7) it is $Q_{\mathrm{L,F}}=U_{\mathrm{F}}\left(A-A_{\mathrm{B}}\right)=JA-U_{\mathrm{B}}A_{\mathrm{B}}$ so that we obtain with $Q_{\mathrm{L}}=J_{\mathrm{L}}A$ from Eq. (9) the result

$$\alpha_{\mathrm{Q}}=\frac{J_{\mathrm{L}}A-(JA-U_{\mathrm{B}}A_{\mathrm{B}})}{J_{\mathrm{L}}A}=\frac{U_{\mathrm{B}}A_{\mathrm{B}}-J_{\mathrm{G}}A}{J_{\mathrm{L}}A}=\frac{U_{\mathrm{B}}}{J_{\mathrm{L}}}\left(\frac{A_{\mathrm{B}}}{A}-\varepsilon\right) \tag{10}$$

Then, the mean residence time of the PDD model is

$$\tau_{\mathrm{UC}}^{\mathrm{PDD}}=\left[\frac{C_{\mathrm{cs}}}{\lambda}+\frac{U_{\mathrm{B}}}{J_{\mathrm{L}}}\left(\frac{A_{\mathrm{B}}}{A_{\mathrm{ch}}}-\varepsilon\right)\right]\frac{L_{\mathrm{UC}}}{J}+\left[1-\frac{U_{\mathrm{B}}}{J_{\mathrm{L}}}\left(\frac{A_{\mathrm{B}}}{A_{\mathrm{ch}}}-\varepsilon\right)\right]\frac{L_{\mathrm{UC}}}{U_{\mathrm{F}}} \tag{11}$$

In general $\tau_{\mathrm{UC}}^{\mathrm{PDD}}$ will differ from the hydrodynamic residence time which is

$$\tau_{\mathrm{h}} = \frac{V}{Q_{\mathrm{L}}} = \frac{AL_{\mathrm{UC}}}{AJ_{\mathrm{L}}} = \frac{L_{\mathrm{UC}}}{J_{\mathrm{L}}} \tag{12}$$

In Tab. 2 we list the values of α_{Q} for both values of β. Also given are values for the relative deviation of the mean residence time from the hydrodynamic one. For $\beta = 1$ the relative error is typically about 4 - 9%, whereas it is about 1 - 7% for $\beta = 0.97$. For both values of β, the relative error is larger for the downward flow case C than for the cases with upward flow. While a relative error of the mean residence time below 7% may be acceptable for some cases, we nevertheless disregard this approach. Instead we determine α from the demand that the mean residence time of the PDD model $\tau_{\mathrm{UC}}^{\mathrm{PDD}}$ is equal to τ_{h} which yields

$$\alpha_{\mathrm{h}} = \frac{\tau_{\mathrm{D}} + \tau_{\mathrm{F}} - \tau_{\mathrm{h}}}{\tau_{\mathrm{F}} - \tau_{\mathrm{S}}} \tag{13}$$

The comparison of the values of α_{h} and α_{Q} for the three cases shows that the differences are rather small, see Tab. 2.

(Approximate location for Tab. 2)

In Fig. 6 we compare the PD and PDD model with the numerically evaluated RTD curves for the three cases. The shaded area represents the numerical RTD curve (with the values of $\Delta t_{\mathrm{class}}$ as given in Tab. 1) while the lines represent the PD model and the PDD model for the two different values of β. The main graphs (with linear axes) show that the peaks of the models are clearly lower than the peak of the numerical RTD for case B and C. However, as noted before the peak height of the numerical RTD is very sensitive to the value of $\Delta t_{\mathrm{class}}$. For all three cases, the curves of the PDD model intersect those of the PD model and exhibit a flatter slope at high residence times. This can be seen more clearly in the inset graphics with semi-logarithmic representation of the data. Fig. 6 shows that the slope of the PDD model changes at $t / t_{\mathrm{ref}} \approx 5$. For larger residence times the slope becomes less steep. In the PDD model, the slope of the RTD at large values of t depends on the value of β. For case A and C the value $\beta = 1$ gives better results, while for case B $\beta = 0.97$ is more appropriate.

Overall, the PDD model with the delay time computed by Eq. (5), U_{F} by Eq. (8) (with $d_{\mathrm{B}} = \beta d_{\mathrm{B,max}}$ and $0.97 \le \beta \le 1$) and α_{h} by Eq. (13) is a reasonably good fit to the numerical RTD curve, both at small and large residence times, and both, for co-current upward and downward Taylor flow.

(Approximate location for Fig. 6)

3.2. Modeling the diffusion-free RTD for multiple unit cells

Since Taylor flow consists of a sequence of a large number of unit cells, the single unit cell RTD model alone is at first of limited practical value. The overall goal is, therefore, to develop a model for the RTD of Taylor flow consisting of n unit cells in series. In this section we investigate if the diffusion-free RTD $E_{n\mathrm{UC}}(t)$ for n identical Taylor flow unit cells can be accurately determined from the single unit cell RTD $E_{\mathrm{UC}}(t)$ by a convolution procedure.

3.2.1. Convolution procedure

The RTD has the property to transfer any reactor input signal $C_{\mathrm{in}}(t)$ into a unique output signal $C_{\mathrm{out}}(t)$. Mathematically, this transfer is described by the convolution integral

$$C_{\mathrm{out}}(t) = \int_0^t C_{\mathrm{in}}(t-t')E(t')dt' \equiv C_{\mathrm{in}} * E \qquad (14)$$

If the input signal has the properties of an RTD, then this also holds for the output signal [39]. For a Taylor flow consisting of n identical unit cells we assume that the input signal for the first unit cell is an ideal Dirac delta pulse. In this case the output signal of the first unit cell is equal to $E_{\mathrm{UC}}(t)$. This RTD is the input signal for the second unit cell, whose output signal is then given by the convolution $E_{\mathrm{UC}} * E_{\mathrm{UC}}$. The RTD $E_{n\mathrm{UC}}(t)$ of unit cell $n>1$ is then given by the convolution integral

$$E_{n\mathrm{UC}}(t) = E_{(n-1)\mathrm{UC}}(t) * E_{\mathrm{UC}}(t) = \int_0^t E_{(n-1)\mathrm{UC}}(t-t')E_{\mathrm{UC}}(t')\mathrm{d}t' \qquad (15)$$

Therefore, one can compute the RTD for a series of n unit cells from the RTD of a single unit cell by successive evaluation of $n-1$ convolutions integrals.

3.2.2. PD model and PDD model for multiple unit cells

In this section we present results of the convolution integrals for the PD model and the PDD model and refer to [50] for mathematical details. We emphasize, that the present convolution procedure is performed in the fixed frame of reference, and thus is different from approaches in literature, where the convolution is based on the unit cell RTD in a frame of reference moving with the liquid slug and where, therefore, a transformation is required to obtain the RTD in the fixed frame of reference [26].

For the PD model, the convolution integral for n identical unit cells in series can be evaluated by Laplace transformation which yields

$$E_{n\mathrm{UC}}^{\mathrm{PD}}(t)=\begin{cases} 0 & \text{for } t<n\tau_{\mathrm{D}} \\ \dfrac{(t-n\tau_{\mathrm{D}})^{n-1}}{(n-1)!\,\tau_{\mathrm{S}}^{n}}\exp\left(-\dfrac{t-n\tau_{\mathrm{D}}}{\tau_{\mathrm{S}}}\right) & \text{for } t\geq n\tau_{\mathrm{D}} \end{cases} \tag{16}$$

The mean residence time is $\tau_{n\mathrm{UC}}=n(\tau_{\mathrm{S}}+\tau_{\mathrm{D}})=n\tau_{\mathrm{UC}}$. For $\tau_{\mathrm{D}}=0$ we have $\tau_{\mathrm{UC}}=\tau_{\mathrm{S}}$ and Eq. (16) becomes equivalent to the RTD of a cascade of n identical CSTRs in series. For the PDD model we cannot present the RTD for arbitrary values of n in a closed form. The result for $n=2$ is $E_{2\mathrm{UC}}^{\mathrm{PDD}}(t)=0$ for $t<2\tau_{\mathrm{D}}$ and

$$\begin{aligned} E_{2\mathrm{UC}}^{\mathrm{PDD}}(t)=(t-2\tau_{\mathrm{D}})&\left[\left(\frac{\alpha}{\tau_{\mathrm{S}}}\right)^{2}\exp\left(-\frac{t-2\tau_{\mathrm{D}}}{\tau_{\mathrm{S}}}\right)+\left(\frac{1-\alpha}{\tau_{\mathrm{F}}}\right)^{2}\exp\left(-\frac{t-2\tau_{\mathrm{D}}}{\tau_{\mathrm{F}}}\right)\right] \\ &+\frac{2\alpha(1-\alpha)}{\tau_{\mathrm{S}}-\tau_{\mathrm{F}}}\left[\exp\left(-\frac{t-2\tau_{\mathrm{D}}}{\tau_{\mathrm{S}}}\right)-\exp\left(-\frac{t-2\tau_{\mathrm{D}}}{\tau_{\mathrm{F}}}\right)\right] \end{aligned} \tag{17}$$

for $t\geq 2\tau_{\mathrm{D}}$. The mean residence time is $\tau_{2\mathrm{UC}}^{\mathrm{PDD}}=2\tau_{\mathrm{UC}}^{\mathrm{PDD}}$. The RTD $E_{3\mathrm{UC}}^{\mathrm{PDD}}(t)$ for three unit cells can be found in [50] and is not repeated here due to its complexity. For $\alpha=1$ and any value of n, the RTD of the PDD model becomes equal to that of the PD model in Eq. (16).

In Fig. 7 we compare the RTD from the convolution procedure (both for the PD and PDD model) for case A and B for two and three unit cells with the respective numerical RTD curves. It is evident that the peak value of the model RTD is always lower than the numerical one. While the difference is rather small for case B (cf. Fig. 7 b and d) it is significant for case A (cf. Fig. 7 a and c). Fig. 7 also shows that for the PDD model the peak value of the RTD is very sensitive to the value of β. In the PDD model this peak value is always smaller than in the PD model; therefore both curves intersect at a certain residence time. As compared to the PD model, the PDD model predicts lower RTD values at small time and higher values at large time. Due to this behavior the PDD model provides a much better fit to the long tails of the numerical RTD both for two and three unit cells. The inset graphics in Fig. 7 show, that at high values of t the slope of the numerical RTD is well approximated by the PDD model with a value of $\beta = 1$ for case A, and $\beta = 0.97$ for case B.

We now discuss the residence time where the peak value occurs. From a comparison with the single unit cell RTDs, which are displayed in Fig. 6 a) and b), it is evident that for the convolution-based RTD the location of the peak is shifted towards residence times that are larger than the respective delay time. Interestingly, in the numerical RTD this shift of the maximum toward residence times larger than τ_{D} occurs only for case A (cf. Fig. 7 a and c) but not for case B (cf. Fig. 7 b and d). In comparison to the numerical RTD curves, the location of the RTD maximum obtained by the convolutions of the PD and PDD models is shifted to still larger times. It is expected that this discrepancy even increases for larger numbers of unit cells in series. Thus, estimating the RTD of a channel with n unit cells by convolution of the single unit cell RTD is obviously not appropriate.

(Approximate location for Fig. 7)

Nauman [54] notes that a key assumption in calculating the RTD of flow networks by convolution procedures is that the subsystems are independent so that the time spent in one ‘vessel’ has no influence on the time spent in another vessel. He also remarks, that laminar flow systems routinely

violate this assumption. In Taylor flow a so-called dividing streamline exists for $U_{\mathrm{B}} < U_{\mathrm{L,max}}^{\mathrm{fd}}$, which partitions the liquid in a region with recirculation flow (in the slug and channel center) from one with bypass flow (close to the channel walls) [41]. In this flow pattern, there is no convective transport between the recirculation and the bypass region and mass transfer across the dividing streamline is only by diffusion. The inset in Fig. 2 displays the velocity field and streamlines in a frame of reference moving with the bubble for case C and illustrates the separation of the liquid in regions with bypass and recirculating flow, respectively.

In our method, virtual particles are released in the entire liquid volume of the unit cell. This means that some particles are released in the liquid slug and other ones in the film/bypass flow region. In Fig. 8 we display the trajectories of selected particles for case C. The instant in time is chosen so that the middle of the liquid slug is located at the top of the computational domain. For this instant in time particles are released at various positions within this top plane (the respective positions are given in the figure caption). In Fig. 8 a) the particle trajectories are displayed for $N_{\mathrm{cross}} = 2$ (i.e. two unit cells). The color code at any position along the trajectory indicates the residence time since the particle has been released. As expected, the residence time is largest in the channel corners and close to the channel walls (yielding the tails in the RTD), whereas the residence time of particles released in the channel center is much shorter (and gives rise for the RTD peaks at low values of t in Fig. 3 and Fig. 6). From Fig. 8 a) it is evident that trajectories in the film/bypass region are rather straight and the respective fluid particles move only short distances in lateral direction. However, the trajectories show periodic kinks which are presumably linked with the passing of the bubbles. The trajectories of those particles that are released in the recirculation region (i.e. inside the diving streamline) do not show such kinks but undergo a significant lateral motion. This can be better seen in Fig. 8 b), where the trajectories of six particles released at different positions along the channel diagonal are displayed for $N_{\mathrm{cross}} = 5$ (i.e. five unit cells). It is obvious that the axial movement of the particle is associated with a periodic lateral movement toward the channel centerline and away from it. This is a result of the recirculation pattern within the liquid slug (cf. the inset in Fig. 2). Fig. 8 clearly shows that particles released in either the film/bypass region or the recirculation region always stay within this region and

do not cross the dividing streamline. In the absence of diffusion, particles cannot go from the slug to the film region and vice versa. This behavior is thus well reproduced by our method. Thus, particles that are initially in the liquid slug remain there, and are still in the liquid slug when their residence time is recorded, after they traveled an axial distance corresponding to the length of one or multiple unit cells. Therefore, a particle that is released in the recirculation (bypass) region will be in the recirculation (bypass) region in any unit cell. As a consequence, in the absence of diffusion neighboring Taylor flow unit cells are not independent in the sense of [54], which makes a convolution procedure inappropriate for these conditions.

We finally note that the sizes of the regions with recirculation and bypass flow is variable and depends on the ratio U_{B} / J [55] which itself is a function of the capillary number [41]. Therefore, in future RTD models for multiple unit cells should be developed which account for the independence of the recirculation and bypass region of the liquid phase in Taylor flow in the absence of diffusion and the variable sizes of both regions.

(Approximate location for Fig. 8*)*

4. Conclusions

In this paper, results from detailed numerical simulations of Taylor flow in a square vertical mini-channel are used to develop an improved analytical model for the liquid phase residence time distribution of a diffusion-free tracer in a Taylor flow unit cell in a fixed frame of reference. The unit cell RTD is represented by a compartment model which consists of a plug flow reactor that is in series with two parallel continuous-stirred-tank reactors. The model for the delay time of the RTD (which corresponds to the residence time of the PFR) takes into account whether the velocity in the liquid slug is fully developed (as it is the case in sufficiently long slugs) or not. The two CSTRs represent the recirculating liquid slug and liquid film region, respectively. Both have a different mean residence time

which results in different slopes of the RTD at small and large residence times. It is shown that the new model accurately represents the numerical unit cell RTD for quite different flow conditions.

In practice, not the RTD of the unit cell but that of a Taylor flow consisting of a finite number of unit cells is of interest. In this paper an attempt is made to determine the diffusion-free RTD for two and three unit cells in series from the unit cell RTD by a convolution procedure. The comparison of the convolution based RTD for two and three unit cells with the numerical RTD shows that the agreement is not satisfactory as the time where the RTD has its maximum is significantly overestimated. Thus, the convolution procedure fails to predict the RTD of multiple unit cells from that of the single unit cell. This failure is attributed to the separation of the liquid slug in a recirculation and a bypass region by the dividing streamline and the independence of both regions in the absence of diffusion. We conclude that in future RTD models for multiple unit cells should be developed which are based on clear hydrodynamic mechanisms of Taylor flow and explicitly account for this independence. In particular, the model should – in addition to the capillary number dependence of liquid film thickness that is already included in some models – take into account the variable sizes of the recirculation and bypass flow regions as well as the transition to complete bypass flow, which occurs at large capillary numbers. Such a model could then be extended to account for tracer diffusion through the diving streamline and for non-perfect Taylor flow, where the length of the individual Taylor bubbles and liquid slugs is not uniform. While experimental data for the unit cell RTD in Taylor flow are not available in literature, there exist data for single channels that could then be used for model validation.

Acknowledgement

The supports of this work by Sakarya University Scientific Research Foundation (project number 2010-01-06-010) and by the EU Erasmus program (S. Erdogan) are gratefully acknowledged.

References

[1] J.R. Burns, C. Ramshaw, The intensification of rapid reactions in multiphase systems using slug flow in capillaries, Lab Chip, 1 (2001) 10-15.
[2] A. Günther, S.A. Khan, M. Thalmann, F. Trachsel, K.F. Jensen, Transport and reaction in microscale segmented gas-liquid flow, Lab Chip, 4 (2004) 278-286.
[3] V. Haverkamp, V. Hessel, H. Löwe, G. Menges, M.J.F. Warnier, E.V. Rebrov, M.H.J.M. de Croon, J.C. Schouten, M.A. Liauw, Hydrodynamics and mixer-induced bubble formation in micro bubble columns with single and multiple-channels, Chem Eng Technol, 29 (2006) 1015-1026.
[4] K. Jähnisch, M. Baerns, V. Hessel, W. Ehrfeld, V. Haverkamp, H. Löwe, C. Wille, A. Guber, Direct fluorination of toluene using elemental fluorine in gas/liquid microreactors, Journal of Fluorine Chemistry, 105 (2000) 117-128.
[5] B.K.H. Yen, A. Günther, M.A. Schmidt, K.F. Jensen, M.G. Bawendi, A microfabricated gas-liquid segmented flow reactor for high-temperature synthesis: The case of CdSe quantum dots, Angew Chem Int Edit, 44 (2005) 5447-5451.
[6] T. Bauer, R. Guettel, S. Roy, M. Schubert, M. Al-Dahhan, R. Lange, Modelling and simulation of the monolithic reactor for gas-liquid-solid reactions, Chem Eng Res Des, 83 (2005) 811-819.
[7] M.T. Kreutzer, F. Kapteijn, J.A. Moulijn, J.J. Heiszwolf, Multiphase monolith reactors: Chemical reaction engineering of segmented flow in microchannels, Chem Eng Sci, 60 (2005) 5895-5916.
[8] S. Roy, T. Bauer, M. Al-Dahhan, P. Lehner, T. Turek, Monoliths as multiphase reactors: A review, AIChE J, 50 (2004) 2918-2938.
[9] R.E. Albers, M. Nystrom, M. Siverstrom, A. Sellin, A.C. Dellve, U. Andersson, W. Herrmann, T. Berglin, Development of a monolith-based process for H2O2-production: from idea to large-scale implementation, Catal Today, 69 (2001) 247-252.
[10] M.C.J. Bradford, M. Te, A. Pollack, Monolith loop catalytic membrane reactor for Fischer-Tropsch synthesis, Applied Catalysis a-General, 283 (2005) 39-46.
[11] R.M. de Deugd, R.B. Chougule, M.T. Kreutzer, F.M. Meeuse, J. Grievink, F. Kapteijn, J.A. Moulijn, Is a monolithic loop reactor a viable option for Fischer-Tropsch synthesis?, Chem Eng Sci, 58 (2003) 583-591.
[12] R. Guettel, U. Kunz, T. Turek, Reactors for Fischer-Tropsch synthesis, Chem Eng Technol, 31 (2008) 746-754.
[13] W. Liu, J.L. Hu, Y. Wang, Fischer-Tropsch synthesis on ceramic monolith-structured catalysts, Catal Today, 140 (2009) 142-148.
[14] J. Sun, J.X. Ju, L. Ji, L.X. Zhang, N.P. Xu, Synthesis of biodiesel in capillary microreactors, Ind Eng Chem Res, 47 (2008) 1398-1403.
[15] M.T. Kreutzer, A. Günther, K.F. Jensen, Sample dispersion for segmented flow in microchannels with rectangular cross section, Anal Chem, 80 (2008) 1558-1567.
[16] T.C. Thulasidas, M.A. Abraham, R.L. Cerro, Dispersion during bubble-train flow in capillaries, Chem Eng Sci, 54 (1999) 61-76.
[17] R.H. Patrick, T. Klindera, L.L. Crynes, R.L. Cerro, M.A. Abraham, Residence Time Distribution in 3-Phase Monolith Reactor, AIChE J, 41 (1995) 649-657.
[18] A.K. Heibel, P.J.M. Lebens, J.W. Middelhoff, F. Kapteijn, J. Moulijn, Liquid residence time distribution in the film flow monolith reactor, AIChE J, 51 (2005) 122-133.
[19] M.T. Kreutzer, J.J.W. Bakker, F. Kapteijn, J.A. Moulijn, P.J.T. Verheijen, Scaling-up multiphase monolith reactors: Linking residence time distribution and feed maldistribution, Ind Eng Chem Res, 44 (2005) 4898-4913.
[20] A.A. Yawalkar, R. Sood, M.T. Kreutzer, F. Kapteijn, J.A. Moulijn, Axial mixing in monolith reactors: Effect of channel size, Ind Eng Chem Res, 44 (2005) 2046-2057.
[21] J.J.W. Bakker, M.T. Kreutzer, K. de Lathouder, F. Kapteijn, J.A. Moulijn, S.A. Wallin, Hydrodynamic properties of a novel 'open wall' monolith reactor, Catal Today, 105 (2005) 385-390.

[22] R. Kulkarni, R. Natividad, J. Wood, E.H. Stitt, J.M. Winterbottom, A comparative study of residence time distribution and selectivity in a monolith CDC reactor and a trickle bed reactor, Catal Today, 105 (2005) 455-463.
[23] S. Lohse, B.T. Kohnen, D. Janasek, P.S. Dittrich, J. Franzke, D.W. Agar, A novel method for determining residence time distribution in intricately structured microreactors, Lab Chip, 8 (2008) 431-438.
[24] F. Trachsel, A. Günther, S. Khan, K.F. Jensen, Measurement of residence time distribution in microfluidic systems, Chem Eng Sci, 60 (2005) 5729-5737.
[25] W. Salman, P. Angeli, A. Gavriilidis, Sample pulse broadening in Taylor flow microchannels for screening applications, Chem Eng Technol, 28 (2005) 509-514.
[26] W. Salman, A. Gavriilidis, P. Angeli, Axial mass transfer in Taylor flow through circular microchannels, AIChE J, 53 (2007) 1413-1428.
[27] M. Muradoglu, A. Günther, H.A. Stone, A computational study of axial dispersion in segmented gas-liquid flow, Phys Fluids, 19 (2007) 072109.
[28] M. Muradoglu, Axial dispersion in segmented gas-liquid flow: Effects of alternating channel curvature, Phys Fluids, 22 (2010) 122106.
[29] A. Cantu-Perez, S. Barrass, A. Gavriilidis, Residence time distributions in microchannels: Comparison between channels with herringbone structures and a rectangular channel, Chem Eng J, 160 (2010) 834-844.
[30] A. Cantu-Perez, S. Barrass, A. Gavriilidis, Hydrodynamics and reaction studies in a layered herringbone channel, Chem Eng J, 167 (2011) 657-665.
[31] V. Hessel, P. Angeli, A. Gavriilidis, H. Löwe, Gas-liquid and gas-liquid-solid microstructured reactors: Contacting principles and applications, Ind Eng Chem Res, 44 (2005) 9750-9769.
[32] R.E. Thiers, A.H. Reed, K. Delander, Origin of the Lag Phase of Continuous-Flow Analysis Curves, Clin Chem, 17 (1971) 42-48.
[33] L.R. Snyder, H.J. Adler, Dispersion in Segmented Flow through Glass Tubing in Continuous-Flow Analysis - Ideal Model, Anal Chem, 48 (1976) 1017-1022.
[34] L.R. Snyder, H.J. Adler, Dispersion in Segmented Flow through Glass Tubing in Continuous-Flow Analysis - Nonideal Model, Anal Chem, 48 (1976) 1022-1027.
[35] H. Pedersen, C. Horvath, Axial-Dispersion in a Segmented Gas-Liquid Flow, Industrial & Engineering Chemistry Fundamentals, 20 (1981) 181-186.
[36] W. Salman, A. Gavriilidis, P. Angeli, A model for predicting axial mixing during gas-liquid Taylor flow in microchannels at low Bodenstein numbers, Chem Eng J, 101 (2004) 391-396.
[37] M. Muradoglu, H.A. Stone, Mixing in a drop moving through a serpentine channel: A computational study, Phys Fluids, 17 (2005) 073305.
[38] M. Wörner, B. Ghidersa, A. Onea, A model for the residence time distribution of bubble-train flow in a square mini-channel based on direct numerical simulation results, Int J Heat Fluid Flow, 28 (2007) 83-94.
[39] O. Levenspiel, Chemical reaction engineering, 3rd ed., John Wiley & Sons, Hoboken, NJ, 1999.
[40] E.B. Nauman, Residence time theory, Ind Eng Chem Res, 47 (2008) 3752-3766.
[41] T.C. Thulasidas, M.A. Abraham, R.L. Cerro, Flow patterns in liquid slugs during bubble-train flow inside capillaries, Chem Eng Sci, 52 (1997) 2947-2962.
[42] W. Sabisch, Dreidimensionale numerische Simulation der Dynamik von aufsteigenden Einzelblasen und Blasenschwärmen mit einer Volume-of-Fluid-Methode, in: Forschungszentrum Karlsruhe Wissenschaftliche Berichte, FZKA 6478, 2000.
[43] W. Sabisch, M. Wörner, G. Grötzbach, D.G. Cacuci, 3D volume-of-fluid simulation of a wobbling bubble in a gas-liquid system of low Morton number, in, 2001.
[44] B.E. Ghidersa, M. Wörner, D.G. Cacuci, Exploring the flow of immiscible fluids in a square vertical mini-channel by direct numerical simulation, Chem Eng J, 101 (2004) 285-294.
[45] M.C. Öztaskin, M. Wörner, H.S. Soyhan, Numerical investigation of the stability of bubble train flow in a square minichannel, Phys Fluids, 21 (2009) 042108.

[46] F. Özkan, M. Wörner, A. Wenka, H.S. Soyhan, Critical evaluation of CFD codes for interfacial simulation of bubble-train flow in a narrow channel, Int J Numer Meth Fluids, 55 (2007) 537-564.
[47] Ö. Keskin, M. Wörner, H.S. Soyhan, T. Bauer, O. Deutschmann, R. Lange, Viscous co-current downward Taylor flow in a square mini-channel, AIChE Journal, 56 (2010) 1693-1702.
[48] O. Levenspiel, J.C.R. Turner, Interpretation of Residence-Time Experiments, Chem Eng Sci, 25 (1970) 1605-1609.
[49] E.B. Nauman, Residence Time Distribution for Laminar-Flow in Helically Coiled Tubes, Chem Eng Sci, 32 (1977) 287-293.
[50] S. Erdogan, M. Wörner, Numerical Investigation and Analytical Modeling of Liquid Phase Residence Time Distribution for Bubble Train Flow in a Square Mini-Channel, Forschungszentrum Karlsruhe in der Helmholtz-Gemeinschaft Wissenschaftliche Berichte, FZKA 7490 (2009).
[51] R.K. Shah, A.L.j.a. London, Laminar flow forced convection in ducts: a source book for compact heat exchanger analytical data, Academic Press, New York, 1978.
[52] A. Tsoligkas, M.J.H. Simmons, J. Wood, Influence of orientation upon the hydrodynamics of gas-liquid flow for square channels in monolith supports, Chem Eng Sci, 62 (2007) 4365-4378.
[53] R.S. Abiev, Simulation of the slug flow of a gas-liquid system in capillaries, Theor Found Chem Eng, 42 (2008) 105-117.
[54] E.B. Nauman, Mixing Effects on Reactor Modeling and Scaleup .3. Residence Time Distributions and Micromixing, Chem Eng Commun, 8 (1981) 53-131.
[55] S. Kececi, M. Wörner, A. Onea, H.S. Soyhan, Recirculation time and liquid slug mass transfer in co-current upward and downward Taylor flow, Catal Today, 147 (2009) S125-S131.

Figure captions

Fig. 1: Sketch of differential RTD curve for a compartment model consisting of a PFR and CSTR in series (PD model).

Fig. 2: Illustration of the influence of Δt_{class} on the numerical RTD curve for case C. The inset shows the computed bubble shape and velocity field in the vertical mid plane in a frame of reference moving with the bubble (left half: streamlines, right half: velocity vectors).

Fig. 3: Comparison of numerical unit cell RTD with the WGO model for case C. The dashed vertical line indicates the bubble break-through time.

Fig. 4: Wall-normal profiles of magnitude of axial velocity in a horizontal cross-section through the middle of the liquid slug for case A, B, and C. For each case the velocity profile is normalized by the respective bubble velocity. The horizontal lines denote the normalized maximum velocity of a fully developed Poiseuille profile for each case.

Fig. 5: Sketch of differential RTD curve for a compartment model consisting of a PFR that is in series with two parallel CSTRs (PDD model).

Fig. 6: Comparison of numerical unit cell RTD for cases A (a), B (b), and C (c) with the PD model and the PDD model for $\beta = 1$ and $\beta = 0.97$.

Fig. 7: Comparison of numerical RTD curves for case A (a, c) and B (b, d) with the PD model and the PDD model for two (a, b) and three (c, d) unit cells in series.

Fig. 8: Visualization of particle trajectories in fixed frame of reference for case C. The bubble shape corresponds to an instant in time when the middle of the liquid slug it located at the top of the computational domain. Trajectories of particles released at selected positions within this plane are shown; the respective cell indices (*i*,*k*) are (4,4), (8,8), (12,12), (16,16), (20,20), (24,24), (4,24), (8,24), (12,24), (16, 24), (4,14), (8,16), (12,18), (16,20), (20,22). a) Trajectories of the entire particle set are displayed for $N_{cross} = 2$. Each trajectory is colored by the dimensionless residence required to reach this position. b) Only the trajectories of particles released in the channel diagonal are shown for $N_{cross} = 5$. The color has no specific meaning but serves to distinguish the different trajectories.

Figures

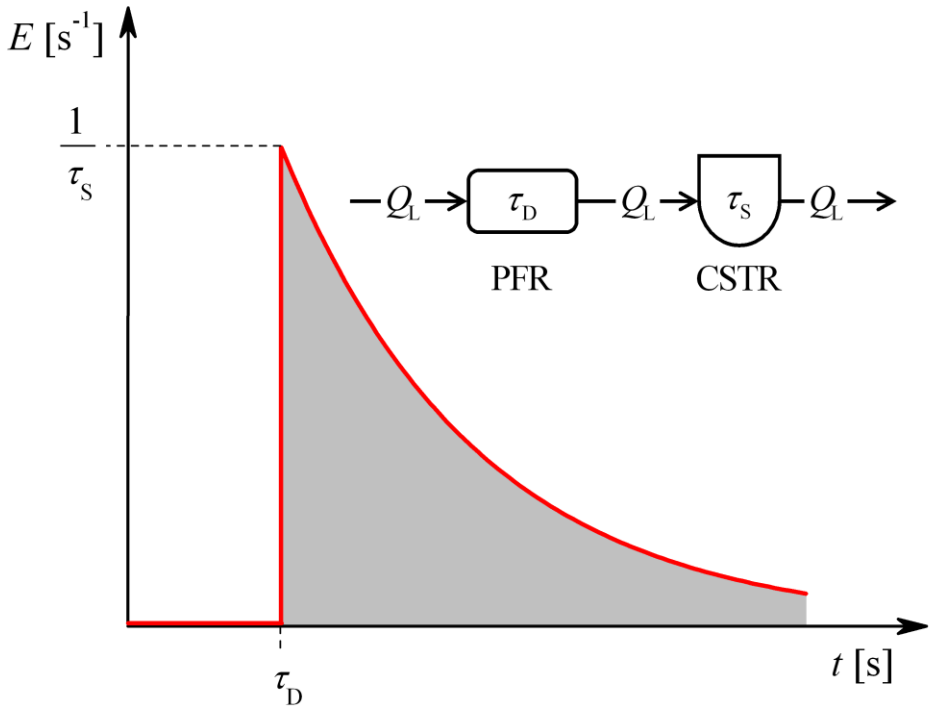

Fig. 1: Sketch of differential RTD curve for a compartment model consisting of a PFR and CSTR in series (PD model).

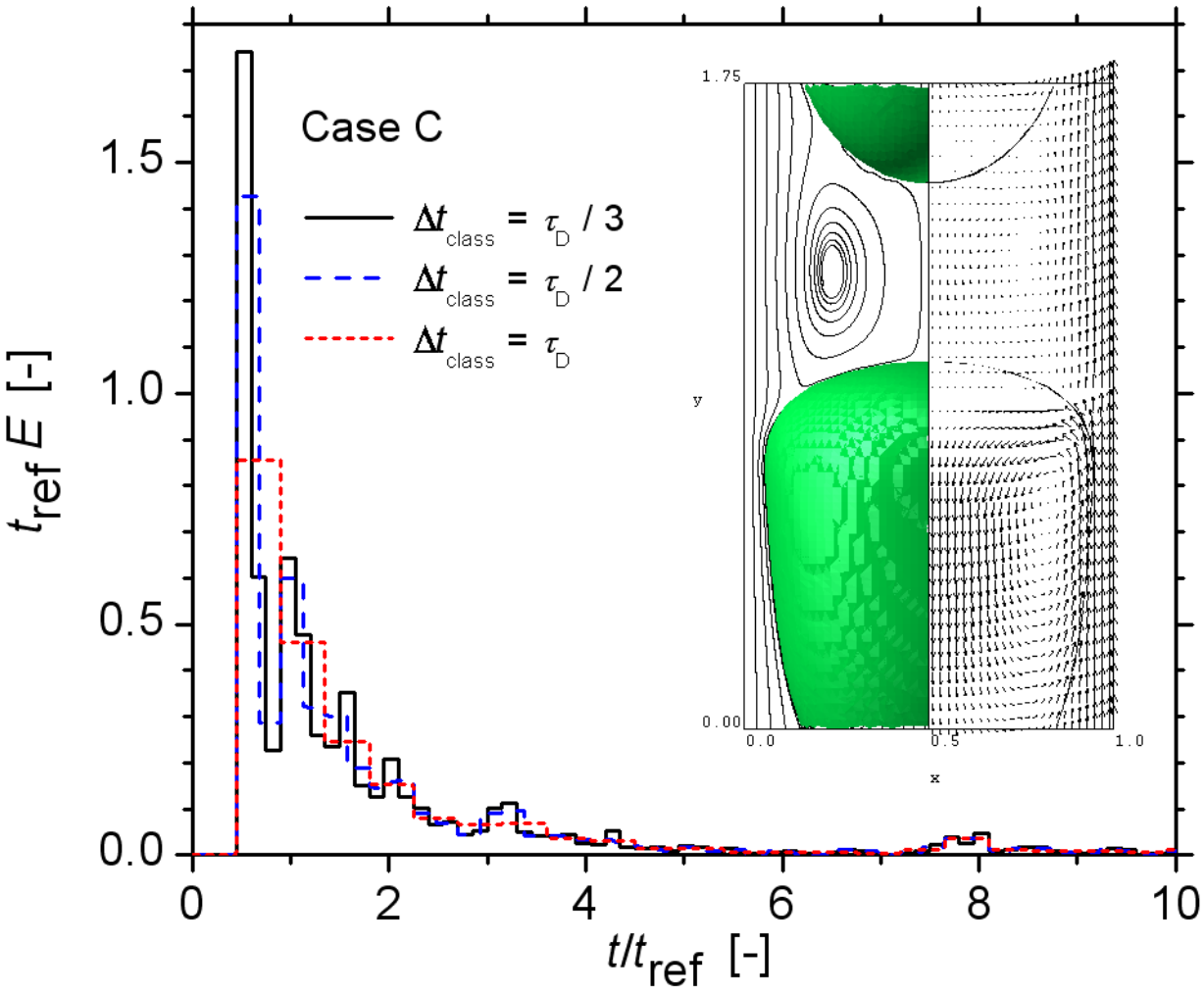

Fig. 2: Illustration of the influence of Δt_{class} on the numerical RTD curve for case C. The inset shows the computed bubble shape and velocity field in the vertical mid plane in a frame of reference moving with the bubble (left half: streamlines, right half: velocity vectors).

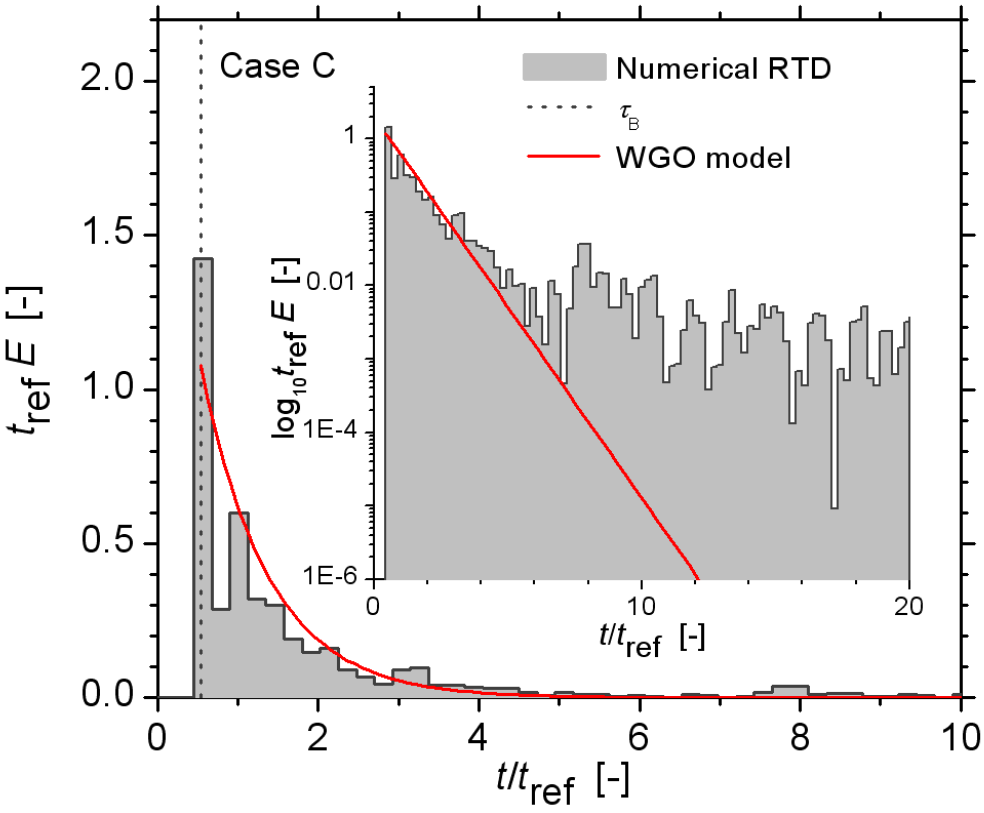

Fig. 3: Comparison of numerical unit cell RTD with the WGO model for case C. The dashed vertical line indicates the bubble break-through time.

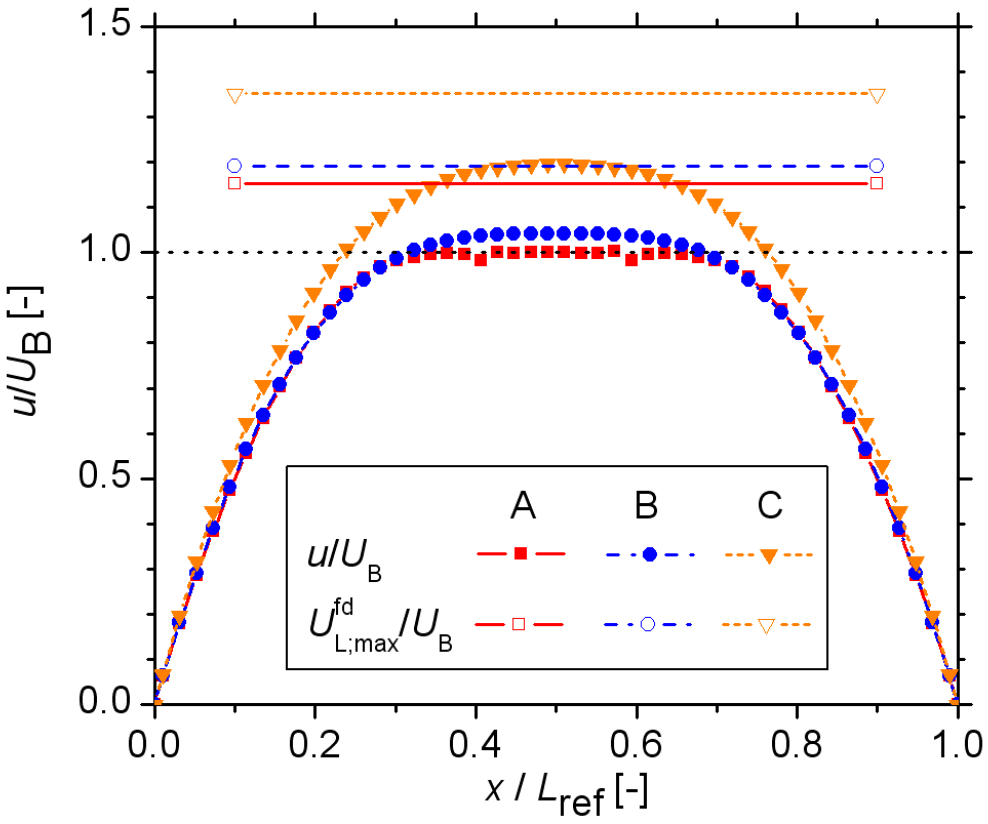

Fig. 4: Wall-normal profiles of magnitude of axial velocity in a horizontal cross-section through the middle of the liquid slug for case A, B, and C. For each case the velocity profile is normalized by the respective bubble velocity. The horizontal lines denote the normalized maximum velocity of a fully developed Poiseuille profile for each case.

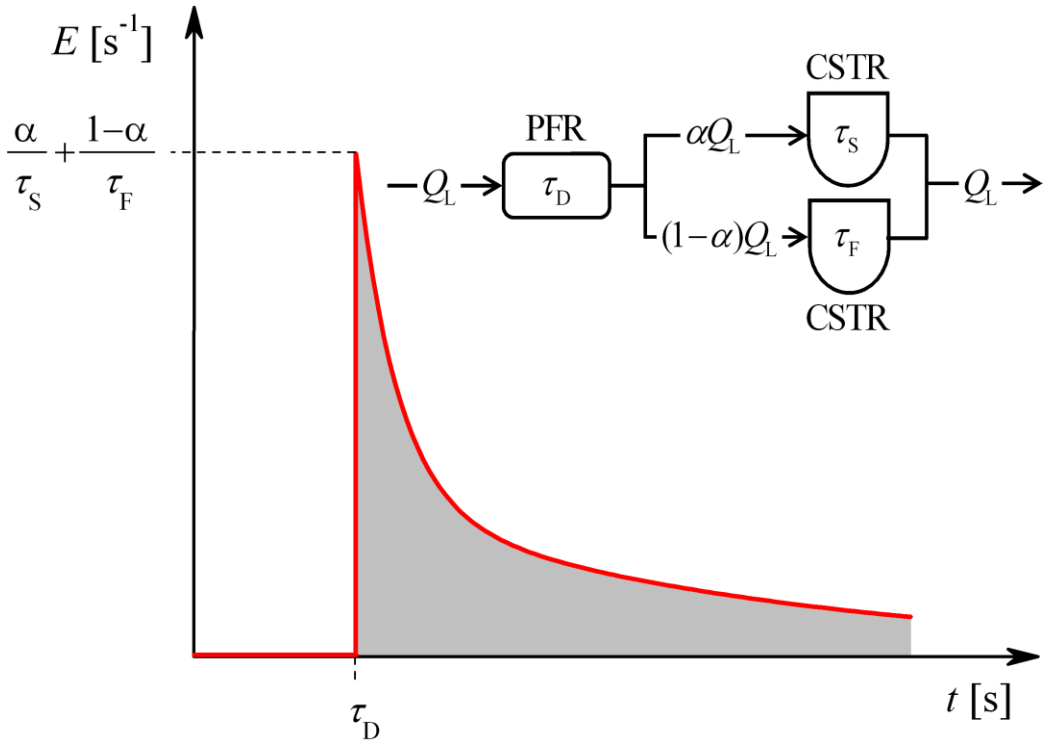

Fig. 5: Sketch of differential RTD curve for a compartment model consisting of a PFR that is in series with two parallel CSTRs (PDD model).

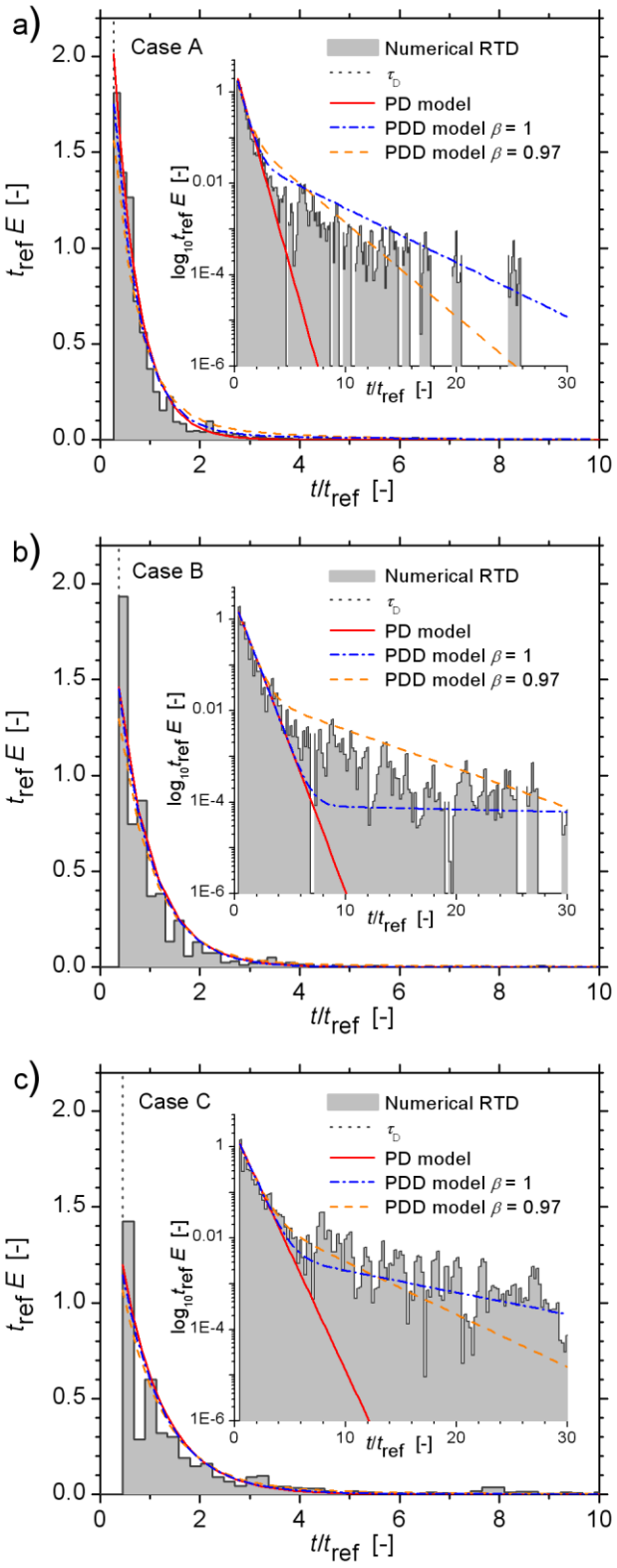

Fig. 6: Comparison of numerical unit cell RTD for cases A (a), B (b), and C (c) with the PD model and the PDD model for $\beta = 1$ and $\beta = 0.97$.

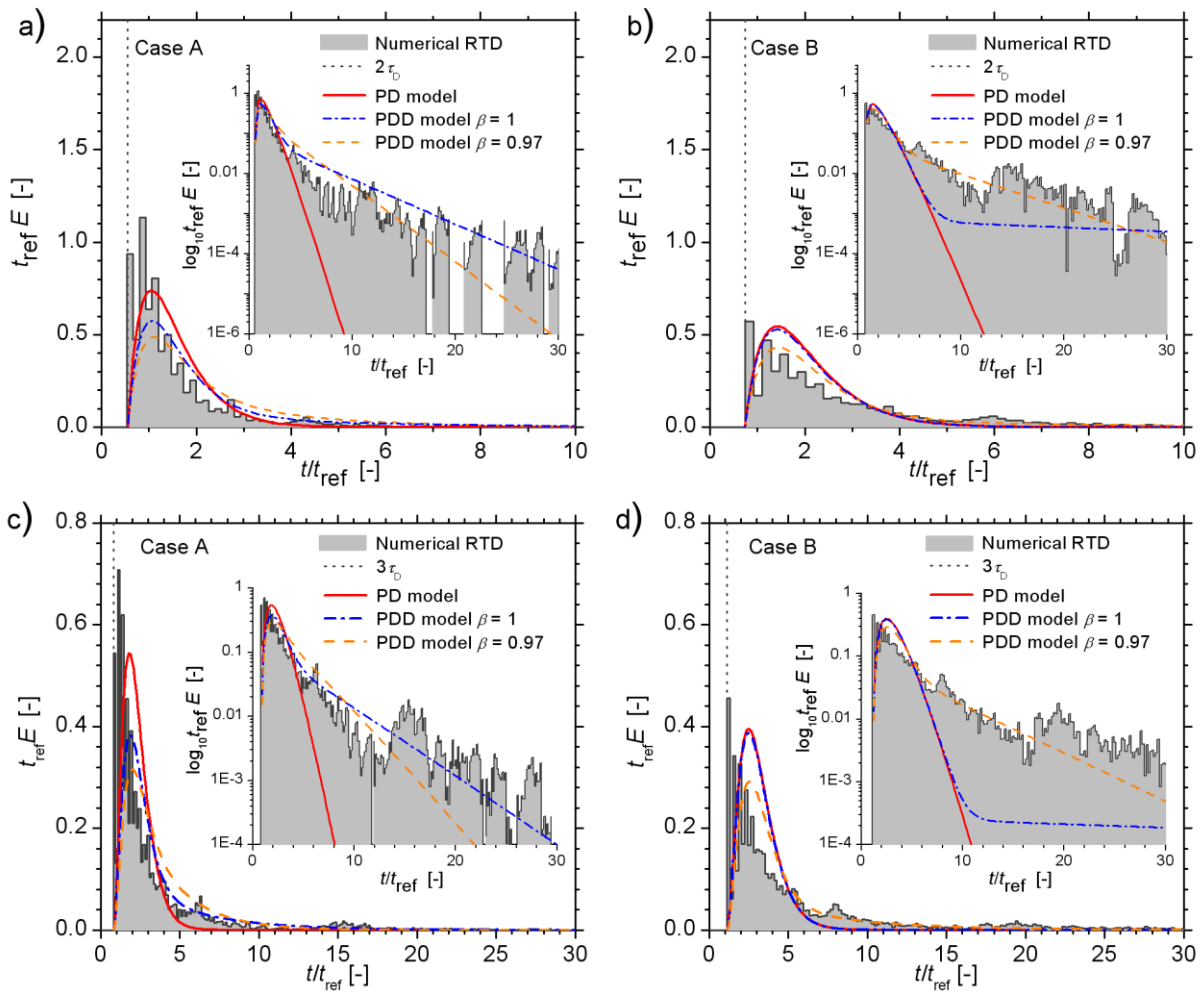

Fig. 7: Comparison of numerical RTD curves for case A (a, c) and B (b, d) with the PD model and the PDD model for two (a, b) and three (c, d) unit cells in series.

a) b)

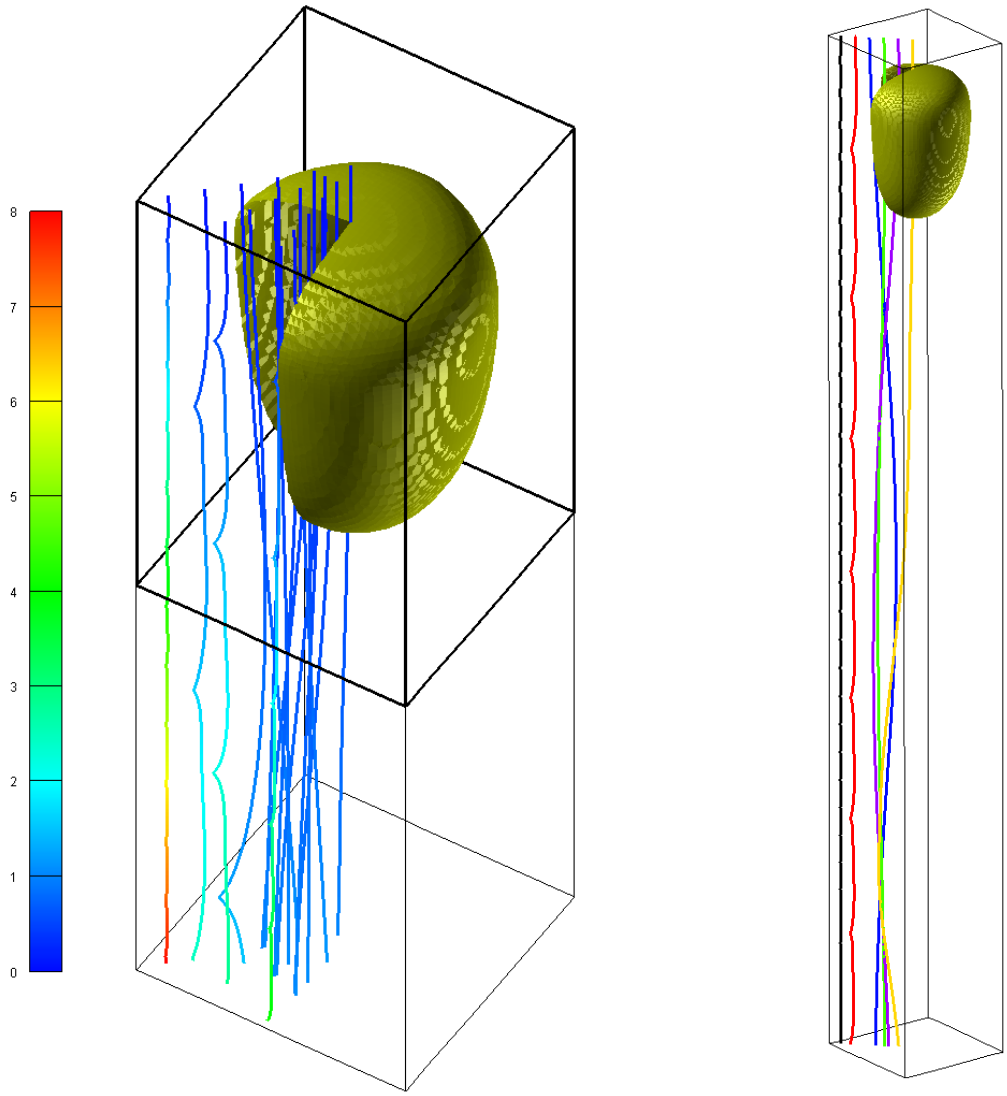

Fig. 8: Visualization of particle trajectories in fixed frame of reference for case C. The bubble shape corresponds to an instant in time when the middle of the liquid slug it located at the top of the computational domain. Trajectories of particles released at selected positions within this plane are shown; the respective cell indices (*i*,*k*) are (4,4), (8,8), (12,12), (16,16), (20,20), (24,24), (4,24), (8,24), (12,24), (16, 24), (4,14), (8,16), (12,18), (16,20), (20,22). a) Trajectories of the entire particle set are displayed for $N_{cross} = 2$. Each trajectory is colored by the dimensionless residence required to reach this position. b) Only the trajectories of particles released in the channel diagonal are shown for $N_{cross} = 5$. The color has no specific meaning but serves to distinguish the different trajectories.

Table captions

Tab. 1: Hydrodynamic parameters of the numerical simulations of Taylor flow.

Tab. 2: Parameter values of the PDD model for the different cases.

Tables

Tab. 1: Hydrodynamic parameters of the numerical simulations of Taylor flow.

Case	A	B	C
Flow direction	Upward	Upward	Downward
L_{UC} / d_h	1	1.5	1.75
U_B / U_{ref}	3.66	3.86	3.25
U_L / U_{ref}	1.20	1.37	1.53
J / U_{ref}	2.02	2.19	2.09
$d_{B,max} / d_h$	0.809	0.849	0.891
L_S / d_h	0.064	0.292	0.480
τ_h / t_{ref}	1.245	1.635	1.708
τ_B / t_{ref}	0.273	0.389	0.539
τ_S / t_{ref}	0.497	0.684	0.836
$U_{L,max} / U_{ref}$	3.66	4.02	3.89
$\lambda = U_{L,max} / U_{L,max}^{fd}$	0.867	0.876	0.879
τ_D / t_{ref}	0.273	0.373	0.450
Re_B	3.86	4.06	3.42
Ca	0.21	0.22	0.19
$\Delta t_{class} / t_{ref}$	0.133	0.186	0.225

Tab. 2: Parameter values of the PDD model for the different cases.

Case	$\beta = 1$					$\beta = 0.97$				
	$\frac{U_F}{U_{ref}}$	$\frac{\tau_F}{t_{ref}}$	α_Q	$\frac{\tau_{UC}^{\alpha_Q} - \tau_h}{\tau_h}$	α_h	$\frac{U_F}{U_{ref}}$	$\frac{\tau_F}{t_{ref}}$	α_Q	$\frac{\tau_{UC}^{\alpha_Q} - \tau_h}{\tau_h}$	α_h
A	0.274	3.65	0.834	3.8%	0.849	0.473	2.12	0.696	1.4%	0.706
B	0.019	78.0	0.991	7.7%	0.993	0.294	5.10	0.850	5.2%	0.869
C	0.193	9.07	0.929	9.4%	0.949	0.465	3.76	0.812	7.4%	0.855